Applied Physics A (2017) 123:788
https://doi.org/10.1007/s00339-017-1414-3

Applied Physics A
Materials Science & Processing

An atomistic study of the deformation behavior of tungsten nanowires

Shuozhi Xu[1] · Yanqing Su[2] · Dengke Chen[3] · Longlei Li[4]

Received: 9 August 2017 / Accepted: 15 November 2017

Abstract
Large-scale atomistic simulations are performed to study tensile and compressive ⟨112⟩ loading of single-crystalline nanowires in body-centered cubic tungsten (W). Effects of loading mode, wire cross-sectional shape, wire size, strain rate, and crystallographic orientations of the lateral surfaces are explored. Uniaxial deformation of a W bulk single crystal is also investigated for reference. Our results reveal a strong tension–compression asymmetry in both the stress–strain response and the deformation behavior due to different yielding/failure modes: while the nanowires fail by brittle fracture under tensile loading, they yield by nucleation of dislocations from the wire surface under compressive loading. It is found that (1) nanowires have a higher strength than the bulk single crystal; (2) with a cross-sectional size larger than 10 nm, there exists a weak dependence of strength on wire size; (3) when the wire size is equal to or smaller than 10 nm, nanowires buckle under compressive loading; (4) the cross-sectional shape, strain rate, and crystallographic orientations of the lateral surfaces affect the strength and the site of defect initiation but not the overall deformation behavior.

1 Introduction

In the last decade, extensive research has been done to investigate mechanical properties of face-centered cubic (FCC) metallic nanopillars and nanowires [1]. Using in situ mechanical deformation instruments, uniaxial tension and compression tests were performed in single-crystalline pillars in Ni [2], Au [3], Cu [4], and Al [5]. It was found that for all these FCC metals, there exists an inverse power-law dependence between the flow stress and the sample size, regardless of the fabrication technique, implying that this scaling might be universal [6]. Both experiments [7] and simulations [8] confirmed that in an FCC metal, dislocations escape from the pillar/wire surface easily, leaving it in a "dislocation-starved" state and requiring a higher stress to nucleate more dislocations to allow continuous plastic deformation.

Compared with FCC nanowires in which the only plastic carriers are dislocations, nanowires in body-centered cubic (BCC) metals are much less investigated [9, 10]. Three plastic deformation mechanisms have been identified in BCC nanowires: dislocation slip, twinning, and phase transformation [11], resulting in properties distinct from those in FCC systems. For example, the shape memory effects and pseudoelasticity in BCC nanowires are attributed to twinning [12, 13], instead of the size-dependent surface stress as in FCC metals [14]. In terms of the strain hardening and strength, nanowires in BCC systems exhibit a much stronger tension–compression asymmetry than those in FCC metals because of the twinning–antitwinning asymmetry and asymmetric plastic deformation mechanisms associated with dislocation core spreading [15, 16]. Kim et al. [17] showed that this tension–compression asymmetry depends on pillar diameter and crystallographic orientation for BCC Mo. Moreover, the "dislocation-starvation" model does not apply to BCC nanowires, due to the combined effects of the image stress and dislocation core structure [8]; consequently, single-crystalline BCC wires generally exhibit a weaker dependence of the strength on the wire cross-sectional area than their FCC counterparts [18].

Besides the wire size, the effects of the wire shape, strain rate, and crystallographic orientations of the lateral surfaces

✉ Shuozhi Xu
shuozhixu@ucsb.edu

[1] California NanoSystems Institute, University of California, Santa Barbara, Santa Barbara, CA 93106-6105, USA

[2] Department of Mechanical Engineering, University of California, Santa Barbara, Santa Barbara, CA 93106-5070, USA

[3] GWW School of Mechanical Engineering, Georgia Institute of Technology, Atlanta, GA 30332-0405, USA

[4] School of Earth and Atmospheric Sciences, Georgia Institute of Technology, Atlanta, GA 30332-0340, USA

Published online: 21 November 2017

(for the nanowires with a square cross section) are potentially important in the deformation of nanowires. Using the nudged elastic band method, Zhu et al. [19] found that in a single-crystalline Cu nanowire with a square cross section under compression, initial dislocation prefers to nucleate from the 90° sharp corner compared with an atomically flat side surface because of a smaller activation volume in the former. In Cu, nanowires with a circular cross section have a higher Young's modulus and yield stress than those with a square cross section of the same size under both tension and compression [20]. In W, in situ transmission electron microscopy (TEM) experiments showed that under [256] compression, micropillars with a circular cross section have a higher flow stress than those with a square cross section [21]. Using in situ TEM, Jennings et al. [22] showed that the transition diameter between dislocation multiplication via the operation of single-arm sources and dislocation nucleation from the surface becomes smaller at a higher strain rate. Previous MD simulations of Au nanowires with a square cross section showed that the deformation behavior may change if different crystallographic orientations of the lateral surfaces are employed [23]. To the best of our knowledge, the effects of the strain rate and lateral surfaces have not been explored using MD for W nanowires.

In this paper, we perform MD simulations to study the deformation behavior of single-crystalline nanowires in BCC W. In particular, the influences of the loading mode (tension or compression), wire shape (circular or square), wire size (2–70 nm), strain rates (5×10^7–10^9 s^{-1}), and crystallographic orientations of the lateral surfaces for the nanowires with a square cross section are explored. Compared with the previous MD work in which W nanowires with either a square cross section of 2.3 nm by 2.3 nm [12] or a circular cross section with a diameter of 8.5 nm [24] or 40 nm [10] were investigated, the nanowires considered in this paper have a cross-sectional size up to 70 nm [9], accessible by experiments [24, 25].

2 Molecular dynamics simulation method

MD simulations are performed using LAMMPS [26] to study the deformation behavior of a bulk single-crystal (Sect. 3) and single-crystalline nanowires (Sect. 4). In all simulation cells, lattice orientations are $x[110]$, $y[1\bar{1}1]$, and $z[1\bar{1}\bar{2}]$, except in Sect. 4.5 where the effects of crystallographic orientations of the lateral surfaces are explored. A Velocity Verlet algorithm with a time step of 2 fs is employed to update the atomic positions. Each model is first dynamically relaxed for 10,000 steps under isobaric zero stresses at 10 K followed by an energy minimization. Then, a constant engineering strain rate $\dot{\varepsilon} = \pm 10^9\ s^{-1}$ is applied along the z direction until the uniaxial engineering strain ε reaches ± 0.2 or ± 0.25. Lattice defects such as dislocations and twinning are identified by the centrosymmetry parameter (CSP) [27]; local atomic structures are classified by the adaptive common neighbor analysis (a-CNA) [28], which provides superior analysis results compared with the conventional CNA with a fixed cut-off radius. Atomic structures are visualized using OVITO [29]. The interatomic potential developed by Ackland and Thetford [30], which modified the short-range region of the Finnis–Sinclair potential [31], is employed, with a lattice parameter of 3.1652 Å. This potential was shown to predict nanowire deformation results that agree with in situ TEM experiments [24]. The uniaxial engineering stress σ, scaled with the initial cross-sectional area of the undeformed nanowire, is calculated following the virial stress formulation.

3 A bulk single crystal

We first study the deformation behavior of a bulk single crystal by applying periodic boundary conditions (PBCs) along all directions. The cuboid simulation cell, containing 6,711,708 atoms, has a size of 47.45 nm by 47.42 nm by 47.30 nm, as shown in Fig. 1a. Using an NPT ensemble, a constant temperature of 10 K and zero transverse stresses in the x–y plane is maintained during uniaxial deformation along the z direction. Stress–strain curves and snapshots of atomic structures corresponding to the yielding/failure are shown in Figs. 1b and 2, respectively.

Under tensile loading, random point-like defects are homogenously nucleated inside the bulk single crystal on the threshold of yielding; no dislocations are observed (Fig. 2a). These point-like defects are results of reversible local atom displacements, which are not sufficiently large to create point defects such as interstitials and vacancies. Under compressive loading, some planar defects on $(2\bar{2}\bar{3})$ planes are nucleated upon yielding, as shown in Fig. 2b. These defects, not residing on any known slip/twin planes but close to {112} twin planes, are a result of local lattice rotation, similar to the "twinning-like lattice reorientation" found in a previous MD study using a different interatomic potential for W [9]. We remark that these twinning-like planar defects have not been reported in any experimental work in the literature, to the best of our knowledge. It will be shown later that nucleation of these planar defects is not relevant for nanowires under compressive loading. At strains larger than 0.15, dislocations on {110} planes are nucleated from these planar defects to form a complex dislocation network. Overall, a strong tension–compression asymmetry is exhibited in terms of both stress–strain response and defect nucleation in a bulk single crystal. At a strain of 0.2, a post-processing based on a-CNA [28] shows that 8.3% (tension) and 0.3% (compression) of all atoms are of FCC local structures. Phase

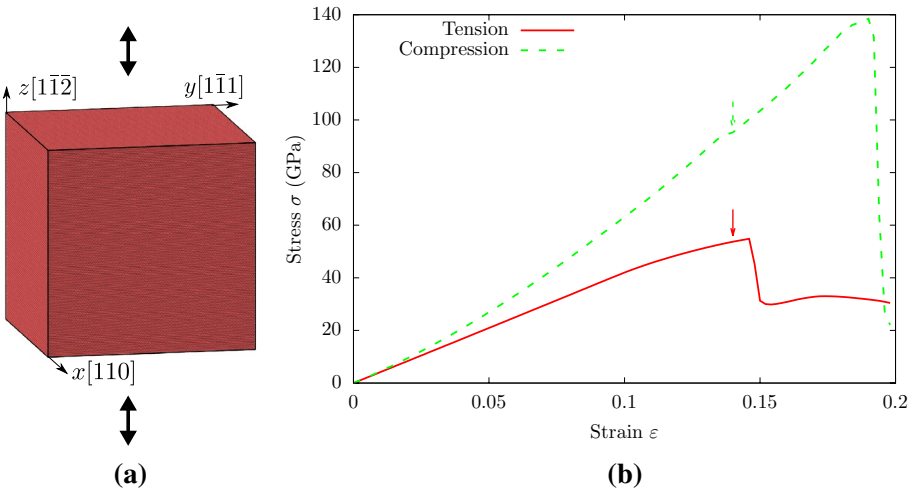

Fig. 1 **a** Simulation cell used to study the deformation behavior of a W bulk single crystal. **b** Stress–strain curves of the bulk single crystal under tension and compression along the z direction

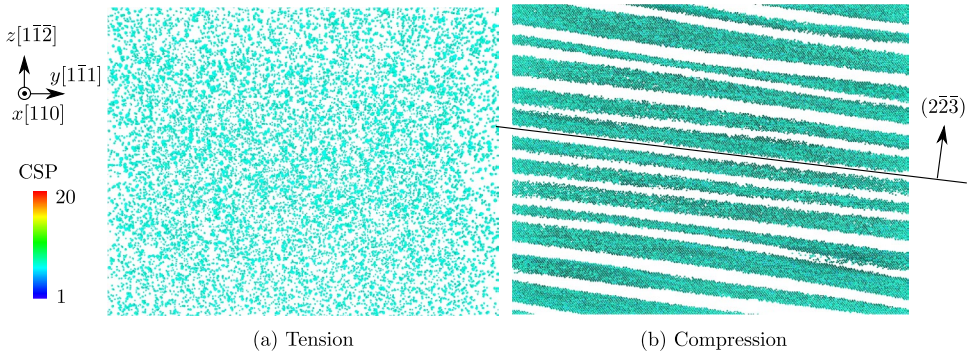

Fig. 2 Snapshots of atomic structures on the threshold of yielding in a W bulk single crystal under **a** tension and **b** compression. Atoms are colored by CSP [27]; those with a CSP smaller than 1 are deleted

transformation from BCC to FCC was also observed in the previous MD simulations of uniaxial compression of Fe bulk single crystals [32, 33].

4 Single-crystalline nanowires

All nanowires have either a circular cross section (Fig. 3a) or a square cross section (Fig. 3b), with the same gauge length $L = 141.9$ nm. The nanowires are initially free of defects. PBCs are applied along the central axis of the wires, i.e., the z direction, while other surfaces are assumed traction free. The wire cross-sectional size D (edge length or diameter) ranges from 2 to 70 nm, resulting in models ranging from 37,558 to 44,487,302 atoms, respectively. During uniaxial deformation, a Nosé–Hoover NVT integrator is used to maintain a constant temperature of 10 K.

4.1 Tensile loading

Stress–strain curves of the nanowires under tensile loading are presented in Fig. 4. In the cases of both circular and square cross section, homogeneous point-like defects are

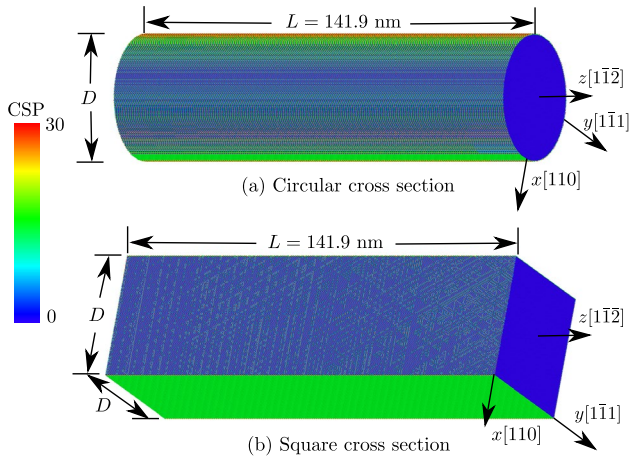

Fig. 3 Simulation cell of nanowires with a **a** circular and **b** square cross section. With a constant initial wire length $L = 141.9$ nm, the initial size of the wire cross-sectional D ranges from 2 to 70 nm. Uniaxial loading is applied along the z direction. Atoms are colored by CSP [27]

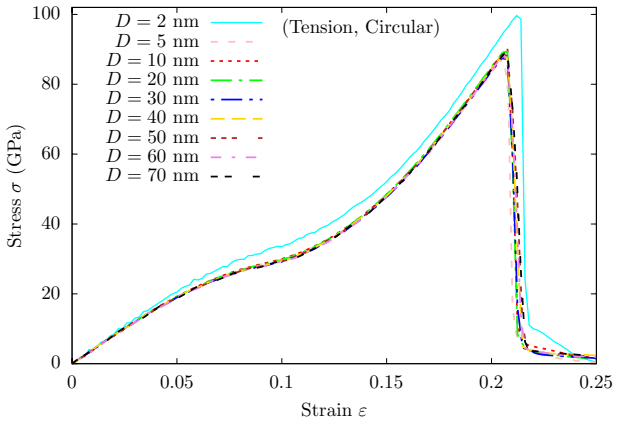

(a) Circular cross section

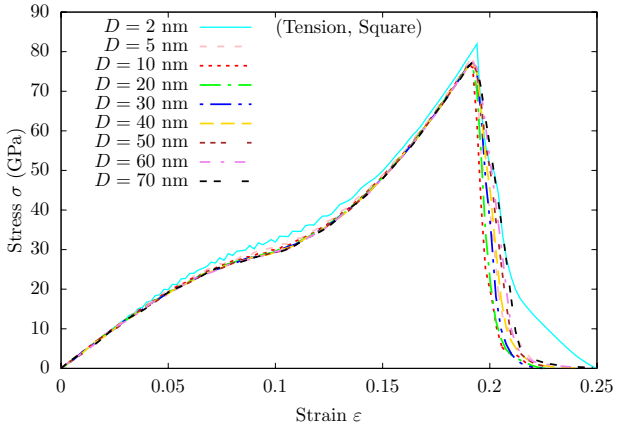

(b) Square cross section

Fig. 4 Stress–strain curves of the nanowires with **a** a circular and **b** a square cross section under tensile loading at 10 K

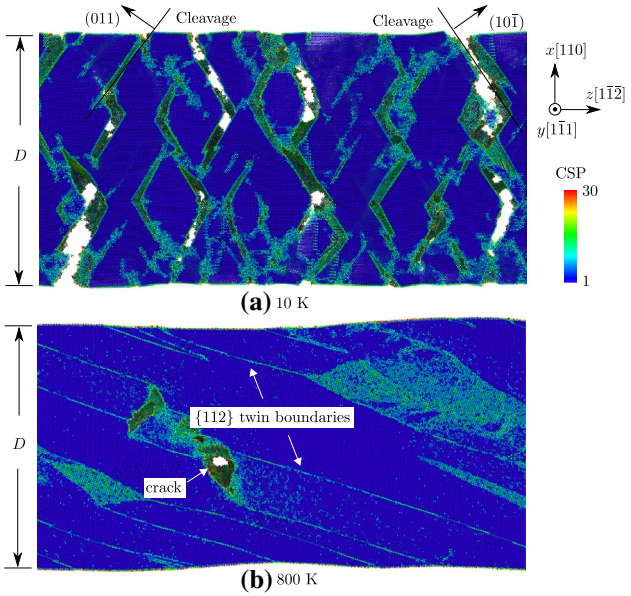

Fig. 5 Snapshots of atomic structure in the nanowire with a circular cross section ($D = 40$ nm) **a** at a tensile strain of 0.252 at 10 K and **b** at a tensile strain of 0.16 at 800 K. In (**a**), cleavage on {110} planes are formed, resulting in failure of the wire. In (**b**), twinning based on {112} planes occurs at the yield point, followed by the formation of cracks along the twin planes. Atoms are colored by CSP [27]

observed inside nanowires up to failure; neither dislocation slip nor twinning is observed for all D, similar to the bulk single crystal. When $D = 40$ nm, a wire fails at a strain of 0.21 due to the cleavage on close-packed {110} planes which have the lowest surface energy among all planes in W [34, 35], as shown in Figs. 5a and 6a. We emphasize that although the nanowires have a relatively large elastic strain limit, they fail in a brittle manner. To explore whether there exists a temperature-dependent brittle-to-ductile transition in nanowire deformation as recently reported by Sainath and Choudhary [36] for BCC Fe, we conduct MD simulations of tensile deformation of two nanowires ($D = 10$ nm and $D = 40$ nm) at 300 and 800 K. Results show that both nanowires fail by brittle fracture at 300 K; at 800 K, however, twinning based on {112} planes occurs at the yield point, followed by the formation of cracks along the twin planes, as shown in Fig. 5b. A systematic study of the temperature effects will be considered in the future.

For the same cross-sectional size D, nanowires with a square cross section have a lower Young's modulus, a lower strength, and a lower flow stress at $\varepsilon = 0.2$ than those with a circular cross section, in agreement with the previous MD simulations in Cu nanowires [19, 20] and twinned W nanowires [9], as well as in situ experiments in W micropillars [21]. The cross-sectional size along the y-axis, D_y, becomes larger than that along the x-axis, D_x, as shown in Fig. 6b, because the {110} surfaces (normal to the x-axis) have a lower surface energy than the {111} surfaces (normal to the y-axis) [34, 35]. Note that the aspect ratio D_y/D_x in the nanowires is larger than that in a bulk single crystal in which only the difference in Poisson's ratio along the two directions takes effect.

4.2 Compressive loading

Stress–strain curves of the nanowires under compressive loading are presented in Fig. 7. The strength for a small diameter D differs markedly from those for a larger D. An investigation into the deformation behavior finds that the nanowires with small D buckle, as shown in Fig. 8a for $D = 5$ nm and Fig. 9a for $D = 10$ nm (i.e., the minimum length-to-diameter aspect ratio for buckling is about 14). Shortly after the buckling, dislocations are initiated at sites on the wire surface with the largest lateral y-displacement; no phase transformation is observed at these sites, in contrast

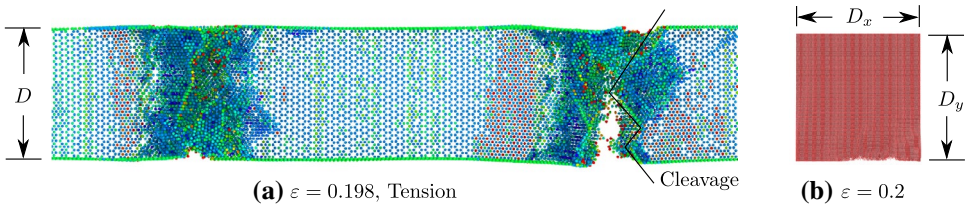

Fig. 6 Snapshots of atomic structures in the nanowire with a square cross section ($D = 10$ nm) under tensile loading at 10 K. Color of atoms and views in (**a**) is the same as in Fig. 5; atoms with a CSP [27] smaller than 1 are removed. In (**a**), the nanowire cleaves on {110} planes. The cross-sectional shape of the nanowires on the x–y plane taken at the mid-z position when $\varepsilon = 0.2$ are given in (**b**)

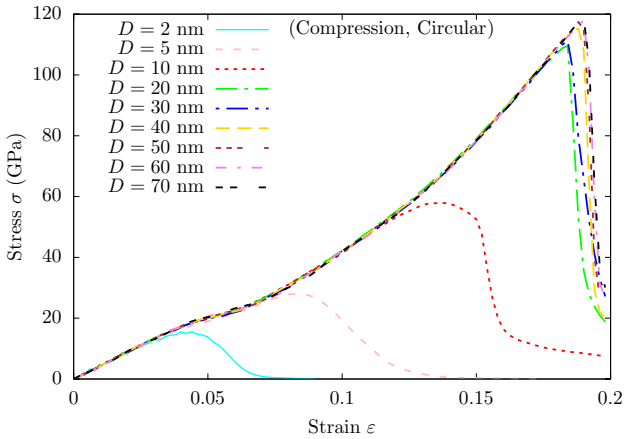

(a) Circular cross section

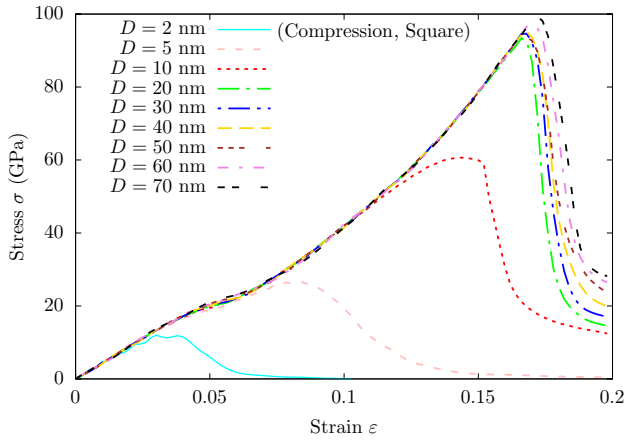

(b) Square cross section

Fig. 7 Stress–strain curves of the nanowires with **a** a circular and **b** a square cross section under compressive loading

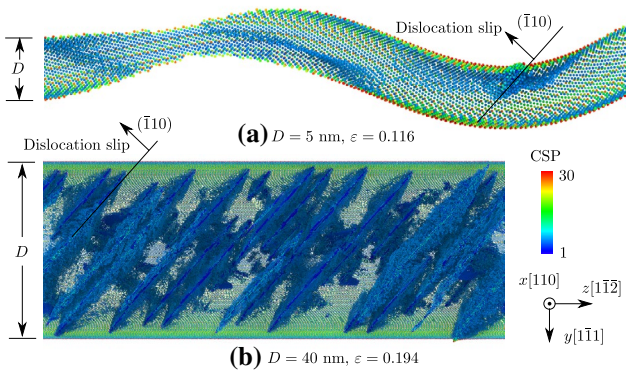

Fig. 8 Snapshots of atomic structures in the nanowires with a circular cross section under compressive loading. In **a**, a nanowire with $D = 5$ nm buckles. In **b**, for nanowires with a larger cross section ($D = 40$ nm), buckling is not observed; instead, dislocations are formed from the wire surface

to a Au nanowire under compressive loading [37]. Similar to tensile loading, the cross-sectional size along the y-axis is larger than that along the x-axis when $\varepsilon = 0.2$, as shown in Fig. 9b. For nanowires with a larger D, as shown in Fig. 8b, buckling is negligible. Unlike the bulk single crystal, there exist no twinning-like planar defects in the nanowires; instead, dislocations on {110} planes are nucleated. Previous MD simulations of a bicrystalline W nanowire showed that under ⟨112⟩ loading, dislocation loops are nucleated and expand from (1) the edge of a pre-embedded twin embryo near the wire surface and (2) the intersection between a free surface and a grain boundary [9, 24]. However, no twin embryo is observed in the present study of the single-crystalline nanowires using the same interatomic potential.

4.3 Tension–compression asymmetry

Figure 10 presents the strength σ_Y as a function of nanowire size D, in cases of tension/compression and circular/square cross section; values of σ_Y for the bulk single crystal are plotted as references. It is found that for the same D, the strength is tension–compression asymmetric in that the compressive loading always has a higher strength than the tensile loading, in agreement with the previous in situ experiments of W nanowires under ⟨100⟩ loading [38]. When $D < 10$ nm, with an decreasing D, the strength of the nanowires increases in tension. The strengths of the nanowires are generally close to or higher than those of the bulk single crystal. When $D \geq 10$ nm, the present work in W and previous MD studies in Fe [39, 40] suggest that the strength of

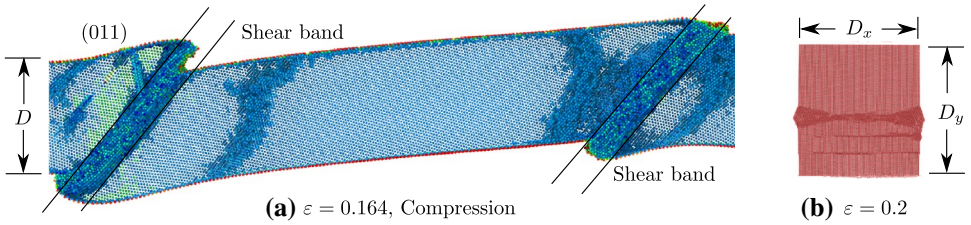

Fig. 9 Snapshots of atomic structures in the nanowire with a square cross section ($D = 10$ nm) under compressive loading. Color of atoms and views in (**a**) is the same as in Fig. 5; atoms with a CSP [27] smaller than 1 are removed. In **a**, shear bands on {110} planes are formed. The cross-sectional shape of the nanowires on the x–y plane taken at the mid-z position when $\varepsilon = 0.2$ are given in (**b**)

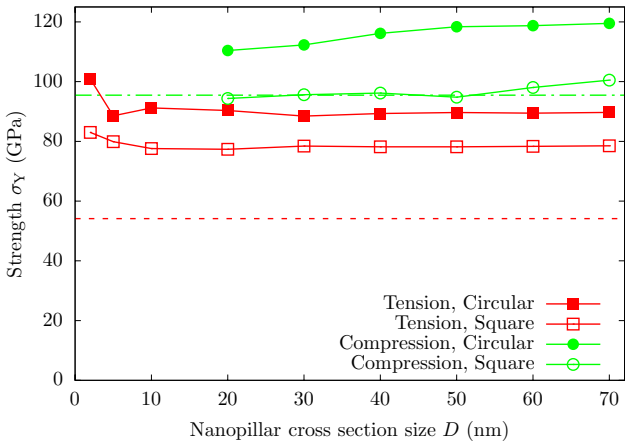

Fig. 10 Strength σ_Y as a function of the nanowire cross-sectional size D, in cases of tension/compression and circular/square cross section. Horizontal dash lines are the strengths of a bulk single crystal for different loading modes, distinguished by color

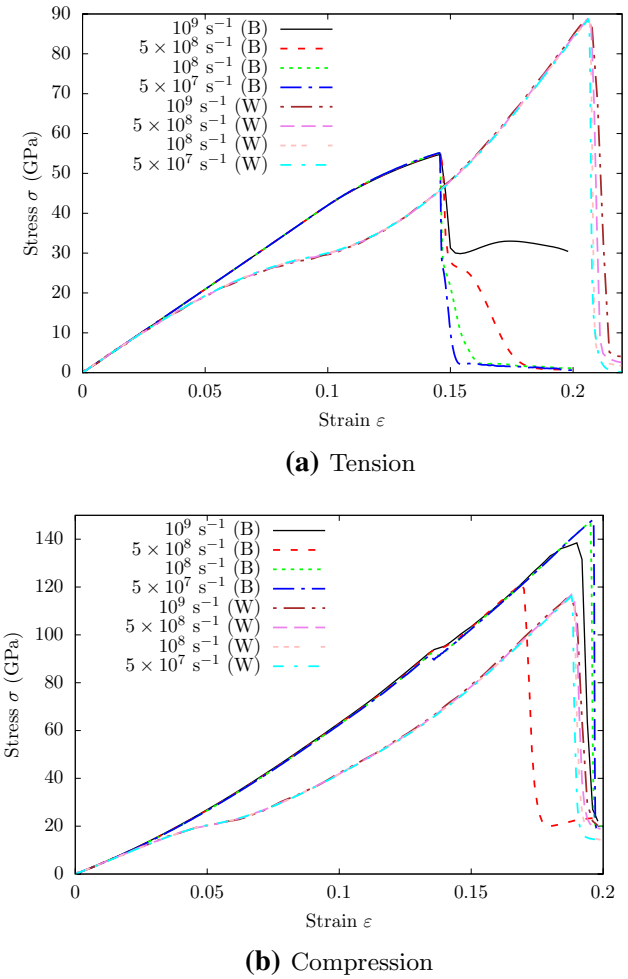

Fig. 11 Stress–strain curves of the bulk single-crystal (B) and the single-crystalline nanowires (W) with a circular cross section ($D = 40$ nm) under **a** tensile and **b** compressive loading

nanowires varies little with D, in contrast to experiments which revealed a log D dependence of the strength [38]. This difference may be attributed to both the much higher strain rate in MD and the lack of dislocation sources in the atomistic models [9].

4.4 Effects of the strain rate

In this section, we explore the effects of the strain rate $\dot{\varepsilon}$ in the deformation behavior of the bulk single crystal and the single-crystalline nanowires with a circular cross section when $D = 40$ nm. Besides $\dot{\varepsilon} = 10^9$ s^{-1}, three lower strain rates—5×10^8 s^{-1}, 10^8 s^{-1}, and 5×10^7 s^{-1}—are employed in both tensile and compressive loading. Figure 11 shows that the stress–strain responses have a weak dependence on $\dot{\varepsilon}$ between 5×10^7 s^{-1} and 10^9 s^{-1}, except for the bulk single crystal under compressive loading. Further analyses of the atomic structure confirm that the defects nucleation and evolution in both the bulk single crystal and the nanowire are almost the same for the four $\dot{\varepsilon}$ examined here. Given the large number of atoms considered in each simulation cell, strain rates that are lower than 5×10^7 s^{-1} are not practical in classical MD simulations, but may be realized using time-scaling atomistic methods [41].

4.5 Effects of the crystallographic orientations of the lateral surfaces for the nanowires with a square cross section

In Fig. 3b, {110} and {111} planes are employed as the lateral surfaces for the nanowires with a square cross section. A question is raised whether employing lateral surfaces of other crystallographic orientations affects the deformation behavior of the nanowires. We remark that most prior atomistic and experimental work only considered one set of lateral surfaces, to the best of our knowledge. In this section, we rotate the x–y plane around the wire central axis, i.e., the z direction, such that nanowires with lateral surfaces of three other sets of crystallographic orientations—$x[24\bar{1}]$-$y[3\bar{1}2]$, $x[7\bar{1}4]$-$y[\bar{1}\bar{3}1]$, and $x[512]$-$y[0\bar{2}1]$—are constructed, as shown in Fig. 12a. Stress–strain curves of the bulk single crystal and the single-crystalline nanowires ($D = 40$ nm) with a circular cross section and a square cross section with lateral surfaces of different crystallographic orientations are presented in Fig. 12b, c. It is found that the crystallographic orientations of the lateral surfaces have a strong influence on the stress–strain response, but not the deformation behavior. We remark that there is no correlation between the strength and surface energies among different sets of crystallographic orientations, suggesting that the yielding/failure may be controlled by detailed atomic structures at the 90° sharp corner of a square cross section [42].

5 Conclusion

In this paper, large-scale MD simulations are performed to study the deformation behavior in single-crystalline nanowires in BCC W. A W bulk single crystal is also deformed in the same way to provide a reference. The stress–strain responses and the deformation behavior are analyzed as a function of the loading mode (tension or compression), the wire cross-sectional shape (circular or square), the wire size (2–70 nm), the strain rate (5×10^7–10^9 s^{-1}), and the

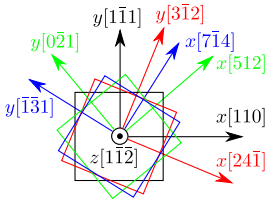

(a)

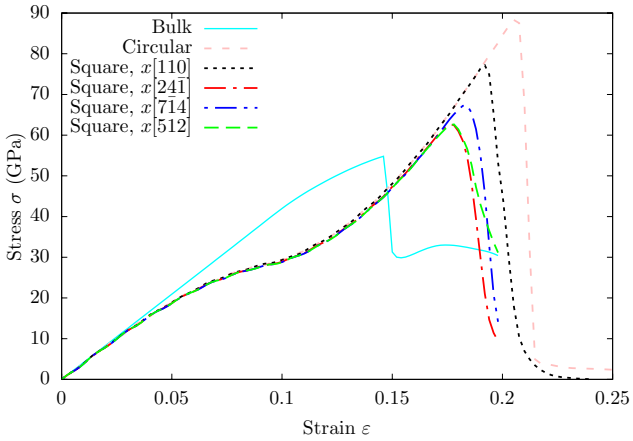

(b) Tension

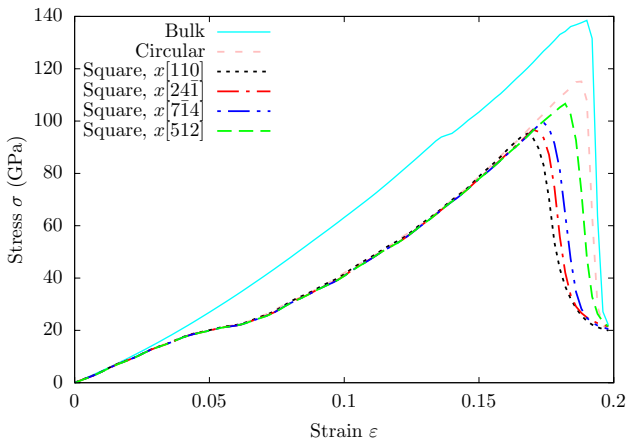

(c) Compression

Fig. 12 **a** Square cross section with lateral x and y surfaces of four different sets of crystallographic orientations, distinguished by color. Stress–strain curves of the bulk single crystal and the single-crystalline nanowires ($D = 40$ nm) with a circular cross section and a square cross section with lateral surfaces of different crystallographic orientations under tensile and compressive loading are presented in (**b**) and (**c**), respectively

crystallographic orientations of the lateral surfaces for the nanowires with a square cross section.

It is found that (1) under tensile loading, the wires fail in a brittle manner by cleaving on close-packed {110} planes, (2) under compressive loading, the nanowires with small cross-sectional size D buckle, while those of a larger size yield due to dislocation slip on {110} planes, (3) when $D \geq 10$ nm, the strength, which is higher than that of a bulk single crystal, exhibits a weak dependence on D under both tensile and compressive loading, in contrast to FCC systems, (4) for the same cross-sectional shape, a strong tension–compression asymmetry is observed in that the strength for compressive loading is higher than that for tensile loading, (5) nanowires with a circular cross section have a higher Young's modulus, a higher strength, and a higher flow stress than those with a square cross section, regardless of the loading mode and the crystallographic orientations of the lateral surfaces, (6) both the cross-sectional shape and the crystallographic orientations of the lateral surfaces affect the initial sites of defect nucleation but not the overall deformation behavior of the nanowires, and (7) the strength has a weak dependence on the strain rate between 5×10^7 s^{-1} and 10^9 s^{-1}, except for the bulk single crystal under compressive loading.

We remark that between the present MD simulations and in situ TEM experiments, there exist quantitative differences that may be attributed in part to the much higher strain rates (5×10^7–10^9 s^{-1}) employed in MD than those (10^{-3}–10^{-1} s^{-1}) in experiments [22], as well as to an assumption of defect-free specimens in MD. Future work includes taking advantage of the accelerated MD approaches [43] to explore deformation behavior of the bulk single crystal and the single-crystalline nanowires at much lower strain rates and with initial dislocation sources such as voids [44–49]. It will also be interesting to investigate whether MD predicts a negligible size dependence of the strain hardening as indicated by experiments [18, 38].

Acknowledgements The work of SX was supported in part by the Elings Prize Fellowship in Science offered by the California Nano-Systems Institute (CNSI) on the UC Santa Barbara campus. SX also acknowledges support from the Center for Scientific Computing from the CNSI, MRL: an NSF MRSEC (DMR-1121053). This work used the Extreme Science and Engineering Discovery Environment (XSEDE), which is supported by National Science Foundation Grant Number ACI-1053575.

References

1. J.R. Greer, J.T.M. De Hosson, Plasticity in small-sized metallic systems: intrinsic versus extrinsic size effect. Prog. Mater. Sci. **56**(6), 654–724 (2011)
2. Z.W. Shan, R.K. Mishra, S.A. Asif, O.L. Warren, A.M. Minor, Mechanical annealing and source-limited deformation in submicrometre-diameter Ni crystals. Nat. Mater. **7**(2), 115–119 (2008)
3. Julia R. Greer, William D. Nix, Nanoscale gold pillars strengthened through dislocation starvation. Phys. Rev. B **73**(24), 245410 (2006)
4. D. Kiener, W. Grosinger, G. Dehm, R. Pippan, A further step towards an understanding of size-dependent crystal plasticity: in situ tension experiments of miniaturized single-crystal copper samples. Acta Mater. **56**(3), 580–592 (2008)
5. K.S. Ng, A.H.W. Ngan, Breakdown of Schmids law in micropillars. Scripta Mater. **59**(7), 796–799 (2008)
6. R. Dou, B. Derby, A universal scaling law for the strength of metal micropillars and nanowires. Scripta Mater. **61**(5), 524–527 (2009)
7. Michael D. Uchic, Dennis M. Dimiduk, Jeffrey N. Florando, William D. Nix, Sample dimensions influence strength and crystal plasticity. Science **305**(5686), 986–989 (2004)
8. Christopher R. Weinberger, Wei Cai, Surface-controlled dislocation multiplication in metal micropillars. Proc. Natl. Acad. Sci. USA **105**(38), 14304–14307 (2008)
9. S. Xu, J.K. Startt, T.G. Payne, C.S. Deo, D.L. McDowell, Size-dependent plastic deformation of twinned nanopillars in body-centered cubic tungsten. J. Appl. Phys. **121**(17), 175101 (2017)
10. S. Xu, S.Z. Chavoshi, Uniaxial deformation of nanotwinned nanotubes in body-centered cubic tungsten. Curr. Appl. Phys. **18**(1), 114–121 (2018)
11. Julia R. Greer, Ju-Young Kim, Michael J. Burek, The in-situ mechanical testing of nanoscale single-crystalline nanopillars. JOM **61**(12), 19–25 (2009)
12. Suzhi Li, Xiangdong Ding, Junkai Deng, Ju Turab Lookman, Xiaobing Ren Li, Jun Sun, Avadh Saxena, Superelasticity in bcc nanowires by a reversible twinning mechanism. Phys. Rev. B **82**(20), 205435 (2010)
13. Ajing Cao, Shape memory effects and pseudoelasticity in bcc metallic nanowires. J. Appl. Phys. **108**(11), 113531 (2010)
14. Wuwei Liang, Min Zhou, Fujiu Ke, Shape memory effect in Cu nanowires. Nano Lett. **5**(10), 2039–2043 (2005)
15. Ju-Young Kim, Julia R. Greer, Tensile and compressive behavior of gold and molybdenum single crystals at the nano-scale. Acta Mater. **57**(17), 5245–5253 (2009)
16. G. Sainath, B.K. Choudhary, Deformation behaviour of body centered cubic iron nanopillars containing coherent twin boundaries. Philos. Mag. **96**(32–34), 3502–3523 (2016)
17. Ju-Young Kim, Dongchan Jang, Julia R. Greer, Crystallographic orientation and size dependence of tension-compression asymmetry in molybdenum nano-pillars. Int. J. Plast. **28**(1), 46–52 (2012)
18. A.S. Schneider, D. Kaufmann, B.G. Clark, C.P. Frick, P.A. Gruber, R. Mnig, O. Kraft, E. Arzt, Correlation between critical temperature and strength of small-scale bcc pillars. Phys. Rev. Lett. **103**(10), 105501 (2009)
19. T. Zhu, J. Li, A. Samanta, A. Leach, K. Gall, Temperature and strain-rate dependence of surface dislocation nucleation. Phys. Rev. Lett. **100**(2), 025502 (2008)
20. Ajing Cao, E. Ma, Sample shape and temperature strongly influence the yield strength of metallic nanopillars. Acta Mater. **56**(17), 4816–4828 (2008)
21. C. Marichal, H. Van Swygenhoven, S. Van Petegem, C. Borca, {110} Slip with {112} slip traces in bcc Tungsten. Sci. Rep. **3**, 2547 (2013)
22. Andrew T. Jennings, Ju Li, Julia R. Greer, Emergence of strain-rate sensitivity in Cu nanopillars: transition from dislocation multiplication to dislocation nucleation. Acta Mater. **59**(14), 5627–5637 (2011)
23. P.A.T. Olsson, H.S. Park, Atomistic study of the buckling of gold nanowires. Acta Mater. **59**(10), 3883–3894 (2011)
24. Jiangwei Wang, Zhi Zeng, Christopher R. Weinberger, Ze Zhang, Ting Zhu, Scott X. Mao, In situ atomic-scale observation of twinning-dominated deformation in nanoscale body-centred cubic tungsten. Nat. Mater. **14**(6), 594–600 (2015)

25. Dongchan Jang, Xiaoyan Li, Huajian Gao, Julia R. Greer, Deformation mechanisms in nanotwinned metal nanopillars. Nat. Nanotech. **7**(9), 594–601 (2012)
26. Steve Plimpton, Fast parallel algorithms for short-range molecular dynamics. J. Comput. Phys. **117**(1), 1–19 (1995)
27. Cynthia L. Kelchner, S.J. Plimpton, J.C. Hamilton, Dislocation nucleation and defect structure during surface indentation. Phys. Rev. B **58**(17), 11085–11088 (1998)
28. Alexander Stukowski, Structure identification methods for atomistic simulations of crystalline materials. Modell. Simul. Mater. Sci. Eng. **20**(4), 045021 (2012)
29. Alexander Stukowski, Visualization and analysis of atomistic simulation data with OVITO–the Open Visualization Tool. Modell. Simul. Mater. Sci. Eng. **18**(1), 015012 (2010)
30. G.J. Ackland, R. Thetford, An improved N-body semi-empirical model for body-centred cubic transition metals. Philos. Mag. A **56**(1), 15–30 (1987)
31. M.W. Finnis, J.E. Sinclair, A simple empirical N-body potential for transition metals. Philos. Mag. A **50**(1), 45–55 (1984)
32. Wei-Wei Pang, Ping Zhang, Guang-Cai Zhang, Xu Ai-Guo, Xian-Geng Zhao, Nucleation and growth mechanisms of hcp domains in compressed iron. Sci. Rep. **4**, 5273 (2014)
33. B.T. Wang, J.L. Shao, G.C. Zhang, W.D. Li, P. Zhang, Molecular dynamics simulations of hcp/fcc nucleation and growth in bcc iron driven by uniaxial compression. J. Phys.: Condens. Matter **21**(49), 495702 (2009)
34. G. Bonny, D. Terentyev, A. Bakaev, P. Grigorev, D. Van Neck, Many-body central force potentials for tungsten. Modell. Simul. Mater. Sci. Eng. **22**(5), 053001 (2014)
35. M.-C. Marinica, L. Ventelon, M.R. Gilbert, L. Proville, S.L. Dudarev, J. Marian, G. Bencteux, F. Willaime, Interatomic potentials for modelling radiation defects and dislocations in tungsten. J. Phys.: Condens. Matter **25**(39), 395502 (2013)
36. G. Sainath, B.K. Choudhary, Atomistic simulations on ductile-brittle transition in ⟨111⟩ BCC Fe nanowires. J. Appl. Phys. **122**(9), 095101 (2017)
37. E. Rabkin, H.S. Nam, D.J. Srolovitz, Atomistic simulation of the deformation of gold nanopillars. Acta Mater. **55**(6), 2085–2099 (2007)
38. Ju-Young Kim, Dongchan Jang, Julia R. Greer, Tensile and compressive behavior of tungsten, molybdenum, tantalum and niobium at the nanoscale. Acta Mater. **58**(7), 2355–2363 (2010)
39. G. Sainath, B.K. Choudhary, T. Jayakumar, Molecular dynamics simulation studies on the size dependent tensile deformation and fracture behaviour of body centred cubic iron nanowires. Comput. Mater. Sci. **104**, 76–83 (2015)
40. G. Sainath, B.K. Choudhary, Molecular dynamics simulations on size dependent tensile deformation behaviour of [110] oriented body centred cubic iron nanowires. Mater. Sci. Eng.: A **640**, 98–105 (2015)
41. Xin Yan, Pradeep Sharma, Time-scaling in atomistics and the rate-dependent mechanical behavior of nanostructures. Nano Lett. **16**(6), 3487–3492 (2016)
42. Eugen Rabkin, David J. Srolovitz, Onset of plasticity in gold nanopillar compression. Nano Lett. **7**(1), 101–107 (2007)
43. Subhendu Chakraborty, Jiaxi Zhang, Somnath Ghosh, Accelerated molecular dynamics simulations for characterizing plastic deformation in crystalline materials with cracks. Comput. Mater. Sci. **121**, 23–34 (2016)
44. S.Z. Xu, Z.M. Hao, Q. Wan, A molecular dynamics study of void interaction in copper. IOP Conf. Ser.: Mater. Sci. Eng. **10**(1), 012175 (2010)
45. S.Z. Xu, Z.M. Hao, Y.Q. Su, Y. Yu, Q. Wan, W.J. Hu, An analysis on nanovoid growth in body-centered cubic single crystalline vanadium. Comput. Mater. Sci. **50**(8), 2411–2421 (2011)
46. S.Z. Xu, Z.M. Hao, Y.Q. Su, W.J. Hu, Y. Yu, Q. Wan, Atomic collision cascades on void evolution in vanadium. Radiat. Eff. Def. Solids **167**(1), 12–25 (2012)
47. Y. Su, S. Xu, On the role of initial void geometry in plastic deformation of metallic thin films: a molecular dynamics study. Mater. Sci. Eng.: A **678**, 153–164 (2016)
48. S. Xu, Y. Su, Nanovoid growth in BCC α-Fe: influences of initial void geometry. Model. Simul. Mater. Sci. Eng. **24**(8), 085015 (2016)
49. S. Xu, Y. Su, D. Chen, L. Li, Plastic deformation of Cu single crystals containing an elliptic cylindrical void. Mater. Lett. **193**, 283–287 (2017)